British
Geological Survey
Expert | Impartial | Innovative

Robust relationships for magnitude conversion of PNR seismicity catalogues

Multihazards and Risk Programme

Open Report OR/20/042

BRITISH GEOLOGICAL SURVEY

Robust relationships for magnitude conversion of PNR seismicity catalogues

B Baptie, R Luckett, A Butcher, M Werner

Keyworth, Nottingham   British Geological Survey   2020

BRITISH GEOLOGICAL SURVEY

The full range of our publications is available from BGS shops at Nottingham, Edinburgh, London and Cardiff (Welsh publications only) see contact details below or shop online at www.geologyshop.com

The London Information Office also maintains a reference collection of BGS publications, including maps, for consultation.

We publish an annual catalogue of our maps and other publications; this catalogue is available online or from any of the BGS shops.

The British Geological Survey carries out the geological survey of Great Britain and Northern Ireland (the latter as an agency service for the government of Northern Ireland), and of the surrounding continental shelf, as well as basic research projects. It also undertakes programmes of technical aid in geology in developing countries.

The British Geological Survey is a component body of UK Research and Innovation.

British Geological Survey offices

Environmental Science Centre, Keyworth, Nottingham NG12 5GG

Tel 0115 936 3100

BGS Central Enquiries Desk

Tel 0115 936 3143
email enquiries@bgs.ac.uk

BGS Sales

Tel 0115 936 3241
email sales@bgs.ac.uk

The Lyell Centre, Research Avenue South, Edinburgh EH14 4AP

Tel 0131 667 1000
email scotsales@bgs.ac.uk

Natural History Museum, Cromwell Road, London SW7 5BD

Tel 020 7589 4090
Tel 020 7942 5344/45   email bgslondon@bgs.ac.uk

Cardiff University, Main Building, Park Place, Cardiff CF10 3AT

Tel 029 2167 4280

Maclean Building, Crowmarsh Gifford, Wallingford OX10 8BB

Tel 01491 838800

Geological Survey of Northern Ireland, Department of Enterprise, Trade & Investment, Dundonald House, Upper Newtownards Road, Ballymiscaw, Belfast, BT4 3SB

Tel 01232 666595
www.bgs.ac.uk/gsni/

Natural Environment Research Council, Polaris House, North Star Avenue, Swindon SN2 1EU

Tel 01793 411500   Fax 01793 411501
www.nerc.ac.uk

UK Research and Innovation, Polaris House, Swindon SN2 1FL

Tel 01793 444000
www.ukri.org

Website www.bgs.ac.uk
Shop online at www.geologyshop.com

Foreword

This report is a product of a study by the British Geological Survey (BGS), Earthnut Ltd. and Avonbank Geophysics Ltd. that was commissioned by the Oil and Gas Authority (OGA) to develop robust relationships between the magnitudes in the catalogues of events recorded by the surface networks and downhole geophone arrays from seismicity induced by hydraulic fracturing operations in the PNR-1z and PNR-2 wells in 2018 and 2019, respectively.

Contents

FIGURES

Summary

In this study we analyse the magnitude estimates from the seismicity catalogues recorded during hydraulic fracturing operations in the PNR-1z and PNR-2 wells in 2018 and 2019, in order to understand the limitations of the different magnitude estimates and to develop robust relationships between the local magnitudes in the catalogue of events recorded by the surface network and the moment magnitudes in the catalogue of events recorded by the downhole geophone arrays. Such relationships are essential to avoid incorrect or biased estimates of seismicity rates and recurrence parameters that describe the exponential frequency magnitude relationship between the number of events and the magnitude of those events. They are also critical for traffic light systems or forecasting methods that use downhole data and important for reliable estimation of source parameters that can provide insights into geomechanics.

We compare the moment magnitudes (Mw) for a subset of events in the PNR-1z and PNR-2 downhole catalogues provided by the operator, Cuadrilla Resources Ltd., with both local magnitudes (ML) and moment magnitudes calculated from surface recordings and find that the moment magnitudes from the PNR-1z and PNR-2 catalogues are not consistent with each other, each having a different relationship with the surface local magnitudes. We also find that referencing the ML-Mw data against existing relationships between surface Mw and ML shows that downhole Mw values are significantly less than the expected value of Mw based on the surface ML. This discrepancy is greater for PNR-1z than for PNR-2.

The overall underestimation of moment magnitude in the downhole catalogues may partly be explained by both the limited dynamic range and frequency response of the 15 Hz geophones used in both PNR-1z and PNR-2, leading to magnitude dependent reductions in recorded amplitudes. The use of two low gain accelerometers with a different frequency response in PNR-2 may also have led to differences between magnitude scaling for PNR-1z and PNR-2. However, we are unable to assess this without access to additional data. Such dependence of Mw on recording instruments is undesirable.

Additionally, we find that moment magnitudes calculated from surface recordings of events during operations in PNR-1z and PNR-2 are greater than the moment magnitudes of the same events determined from the downhole data by the operators. The surface moment magnitudes also broadly agree with those expected using a number of different empirical relationships between ML and Mw. This may also be a result of the limited dynamic range and frequency response of the 15 Hz geophones used in the downhole data acquisition. It may also reflect differences in the method and parameters used by us and the operators to calculate the moment magnitudes using surface and downhole data. Such differences can result in significant differences in magnitudes estimates.

While we find that the magnitudes in the surface catalogue are consistent and reliable, the small number of events recorded means that there is limited overlap between the surface and downhole catalogues, making it difficult to validate the downhole magnitudes and calculate reliable adjustment factors across a wider range of magnitudes.

We correct the moment magnitudes in the downhole catalogues using two different approaches. The first is based on the observed relationship between surface local magnitude and downhole moment magnitude, which is then referenced to an existing relationship between surface moment magnitude and surface local magnitude. The second is based on the observed relationship between surface and downhole moment magnitude. In each case, the corrections result in increases to measured activity rate. However, we obtain different b-values for the two approaches, particularly for PNR-2, where a considerable reduction b-value is observed using the first approach. We suggest this may be the result of using two regressions rather than one. As a result, the second approach may be preferable where surface estimates of moment magnitude are available in sufficient number and quality.

A fuller understanding of these results will require calculation of Mw for both the PNR-1z and PNR-2 downhole catalogues, as well as systematic analysis of the downhole waveform data to understand its limitations.

Given these conclusions we suggest the following recommendations for any future operations.

Operators should assess the possible impact of the type of instrumentation on magnitude determination and provide instrument calibration data so that this can also be assessed independently. This would facilitate a comparison between surface-derived magnitude estimates used for regulatory purposes and downhole-derived magnitude estimates used for monitoring, forecasting and potential hazard mitigation actions.

The methods and parameters used to calculate magnitudes together with amplitude phase data for individual recording sites are made available to enable duplication of results and assessment of uncertainties. To ensure reproducible and transparent magnitudes, these should include the spectral estimation method and associated parameters (e.g. velocity model, density).

Denser networks of surface sensors and improved methods of deployment such as shallow borehole sensors should be used to improve event detection and characterisation. This would also help address the limited completeness of the surface catalogues and ensure that all events around amber light threshold of 0 ML are detected.

Moment magnitudes for both the PNR-1z and PNR-2 downhole catalogues should be recalculated, as well as systematic analysis of the waveform data to understand its limitations.

1 Introduction

Seismicity catalogues are the basic starting point for many studies of both natural and induced seismicity, and contain a parametric description of seismicity in a particular region of space and time with an entry for each event that provides at least a location, origin time, and magnitude. Often, individual catalogues may contain magnitude data that have been determined in different ways, e.g. from broadband waveform inversion (e.g. moment magnitude, Mw) or narrow-band maximum amplitude data (e.g. local magnitude, ML). Similarly, it may be necessary to merge multiple catalogues for different regions in which the magnitudes have been determined in different ways, which can result in highly heterogeneous data.

Any study of seismic hazard critically requires that the magnitude data in the input seismicity catalogues are homogeneous and consistent, which requires robust relationships between different magnitude estimates that allow magnitude data to be converted to the same scale (e.g. Grünthal et al., 2009). Failure to address this issue will result in incorrect or biased estimates of seismicity rates and recurrence parameters that describe the exponential frequency magnitude relationship between the number of events and the magnitude of those events This, in turn, will lead to either under- or over-estimates of seismic hazard. This issue is equally relevant in studies of induced seismicity where attempts to make deterministic forecasts based on cumulative injection volumes (e.g. Verdon & Budge, 2018) or statistical forecasts based on Epidemic Type Aftershock Sequence (ETAS) models (e.g. Mancini et al, 2019) critically depend on robust estimates of seismicity rates and recurrence parameters.

Magnitude conversion relationships are typically empirical scales derived from existing earthquake catalogues. These are often developed for conversion of catalogues compiled by agencies that use local magnitude scales to a common moment magnitude scale that can be used for regional hazard analysis and may only be applicable within certain magnitude ranges (usually higher magnitudes). The relationship between M_L and M_W is often observed to be close to 1:1 for magnitudes greater than 3 M_L (e.g. Fäh et al., 2011; Ottemöller & Sargeant, 2013). There are fewer relationships at lower magnitudes, however, those that exist often use either a quadratic term to fit the data (Edwards et al., 2011; Grünthal et al., 2009) or a low scaling relationship (Munafò et al., 2016). Goertz-Allmann et al. (2011) proposed a piecewise empirical scaling relationship for Switzerland, which uses two different linear M_L and M_W relationships for $M_L < 2$ and $M_L > 4$, with a quadratic relationship bridging the two scales. In general, these relationships demonstrate that M_W becomes progressively larger than M_L as magnitudes decrease.

Regulations for onshore oil and gas (shale gas) exploration in the UK contain specific measures for the mitigation of induced seismicity, including using a 'traffic light' system (TLS) to control whether injection can proceed or not, based on that seismic activity. The critical thresholds for the TLS are defined in terms of local magnitude and require operators to stop hydraulic fracturing if an event with a magnitude of 0.5 ML or above occurs during operations. This limit is significantly lower than the limits for induced seismicity caused by hydraulic fracturing imposed by other regulatory authorities in North America and requires robust estimation of magnitude. Additionally, event magnitudes are generally estimated by averaging measurements from a number of stations to reduce random errors. However, for a small event, the averaging procedure can result in a network magnitude value which is biased high (e.g. Evernden and Kohler, 1976). At those stations where signals fall below the noise, the small signal amplitudes will not be seen. Consequently, only higher amplitude values from other stations are available for use in computing the network average. With the low values missing, this network average is biased high unless a statistical correction is made.

Seismicity induced by hydraulic fracturing operations in both the PNR-1 well in October-December 2018 (Clarke et al., 2019) and the adjacent PNR-2 well in August 2019 was recorded by both a dense network of surface sensors and by downhole geophone arrays. The catalogue of

events recorded using the surface array contains magnitudes given in the local magnitude scale, while the catalogue recorded by the downhole arrays have magnitudes given in a moment magnitude scale. The limited dynamic range and frequency response of the downhole geophones means that magnitude estimates may be unreliable, however, this is poorly quantified by previous analysis. Ideally, moment magnitudes for these events could be either measured from surface data or estimated from the local magnitudes in the catalogue of events recorded by the surface network. However, Mancini et al. (2019) found that existing conversion relationships between moment and local magnitude do not match the observed PNR-1z data well and when applied, they introduce artefacts in the magnitude dataset. As a result, estimates of activity rates and recurrence parameters, as well as extrapolating the observed rates at low magnitudes to rates at higher magnitudes, are subject to greater uncertainty than desirable. Additionally, the relationships between the downhole and surface magnitudes in the PNR-1 data and the PNR-2 data show significant differences, which makes it difficult to compare the data.

The aim of this work is to develop a robust relationship between the local magnitudes in the catalogue of events recorded by the surface network and the moment magnitudes in the catalogue of events recorded by the downhole geophone arrays. This will allow us to determine reliable and consistent moment magnitude estimates for all events in the downhole catalogues, including those events for which the recordings are unreliable as a result of the limited dynamic range of the sensors. This will provide homogeneous catalogues of events for both PNR-1 and PNR-2 that can be used to reduce the uncertainties in the parameters of the frequency magnitude distributions. Finally, it will allow us to determine consistent magnitudes for the PNR-1 and PNR-2 data that can be used to compare the seismicity and make more robust estimates of risks in the future.

2 Data and Exploratory Analysis

The PNR-1z well targets the Bowland shale at a depth of approximately 2,300 m, and runs approximately east-west for 700 m horizontally through the unit. A sliding-sleeve completion method was used, with 41 individual sleeves spaced at intervals of 17.5 m along the well. The hydraulic fracture plan allowed for up to 765 m^3 of fluid per sleeve. A "mini-frac" consisting of a few 10s of m^3 of fluid was pumped prior to each main stage. The sleeves were numbered from 1 to 41 proceeding from the toe (west) to the heel (east) of the well. A total of 16 sleeves were hydraulically fractured with an additional 18 mini-fracs between 16 October 2018 and 17 December 2018.

The sleeves were used in the following order: 1, 2, 3, 12, 13, 14, 18, 22, 30, 31, 32, 37, 38, 39, 40 and 41. The average injected volume for each fracture was 234 m^3 and the maximum injected volume was 431 m^3. No hydraulic fracturing was carried out between 3 November and 4 December as flow-back from the well took place.

The horizontal PNR-2 well runs roughly parallel to the PNR-1Z well and is offset by approximately 200 m. The approach was similar to PNR-1Z, with up to 45 possible hydraulic fracture stages with a planned maximum injected volume of 765 m^3 in any single stage. Operations started on 15 August 2019 and only seven of these stages were completed as operations were suspended following a magnitude of 2.9 ML earthquake on 26 August at 07:30 UTC, almost 72 hours after a hydraulic fracture stage on 23 August. The earthquake was strongly felt locally at distances of up to a few kilometres from the epicenter.

Seismicity during operations in the PNR-1z well was recorded by the operators with a downhole geophone array in the adjacent PNR-2 well. This monitoring setup is shown in Figure 2.1. The geophones were located in the heel of the well resulting in approximate path lengths from the sleeves in PNR-1z of between around 200 to 800 m. The downhole array consisted of 12 Avalon Science Limited Geochain Slim three component geophone tools. The frequency response of the geophones is flat above the corner frequency of 15 Hz, so the amplitude of signals below this

frequency will be systematically underestimated leading to corresponding underestimates in event magnitudes. Similarly, seismicity during operations in the PNR-2 well was recorded by a downhole geophone array in the adjacent PNR-1Z well. Again, the array consisted of 12 three component geophone tools. Geophone and sleeve locations are shown in Figure 2.1. Ten of the geophones were the same Geochain Slim three component geophone tools with a corner frequency of 15 Hz. The two other instruments appear to have been accelerometers with a frequency response that was flat above a corner frequency of 3.0 Hz and a lower gain to enable on-scale recording of larger events, however, we were unable to obtain confirmation of this from the operator.
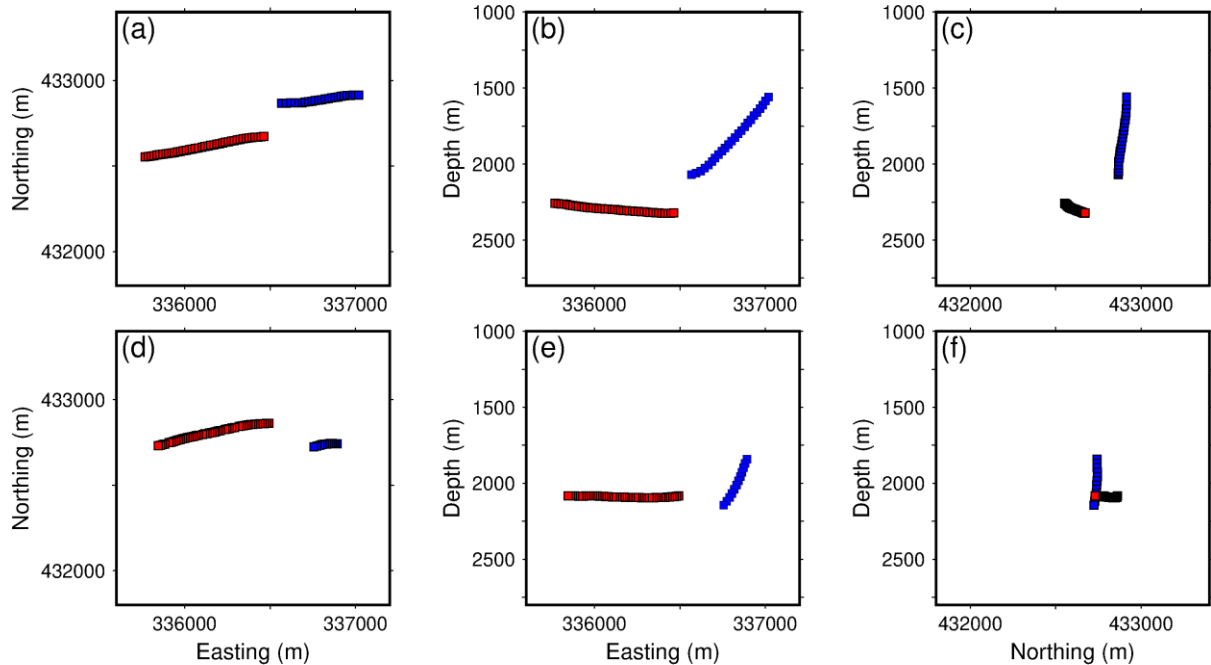
Figure 2.1. Downhole acquisition geometry showing locations of sleeves in well PNR-1z (red squares) and the geophones in PNR-2 (blue squares). (a) plan view, (b) East-West cross-section and (c) North-South cross section.

The geophones recorded almost continuously from the onset of operations in each well, detecting over 38,000 microseismic events from PNR-1z and over 55,000 events from PNR-2. The event catalogues supplied by the operator for the project consist of origin times, locations and magnitudes of the events, as determined by a geophysical processing contractor. No information was available on the method used to locate individual events and the catalogues did not include location uncertainties. The hydraulic fracture plan for PNR-1z (Cuardilla, 2018) gives estimated location accuracies of 37.5 m, while the plan for PNR-2 gives 25 m. More generally, typical location uncertainties for downhole microseismic data are around 10-20 m in depth and slightly larger uncertainties in horizontal location. The downhole catalogues for PNR-1z and PNR-2 contained both moment and local magnitude estimates. No information was available on how the magnitudes were determined or the magnitude uncertainty. We assume that the local magnitudes were calculated using the Luckett et al (2019) relationship. We also assume that the catalogue magnitudes are an average of a number of measurements from different geophones. However, individual amplitudes were not provided for each geophone, so it was not possible to assess possible biases as a result of acquisition geometry. Similarly, although a systematic study of event locations is outside the scope of this report, we note that the acquisition geometry may result in some bias in location estimates, which may propagate into magnitude estimates (Zaliapin and Ben Zion, 2015). We also observe a number of small apparent gaps in the downhole catalogue, when events that were detected by the surface network were not in downhole catalogue. It is unclear what caused these gaps. These gaps included the time period in which the largest event occurred, the magnitude 2.9 ML earthquake on 26 August at 07:30 UTC. We would expect this event to

trigger additional dependent events, which may also be missing from the downhole catalogue, leading to increases in uncertainty.

Surface sensors were deployed at distances of 1.5 to 20 km from the surface position of PNR-1, by Cuadrilla Resources Ltd (the operator), the British Geological Survey (BGS) and the University of Liverpool (Figure 2.2). For operations in PNR-1z, the Cuadrilla network consisted of three-component geophones with a corner frequency of 4.5 Hz and data were recorded with a sampling rate of 200 Hz. For operations in PNR-2, it consisted of Nanometrics Trillium Compact seismometers with a corner period of 20 seconds. The BGS stations consisted of three component Guralp CMG-3ESPC broadband seismometers and Guralp CMG-DM24-3C-EAMU data loggers throughout with a lower corner of 30 sec and a sample rate of 200 Hz. The Liverpool stations used Nanometrics Trillium 240 broadband seismometers.
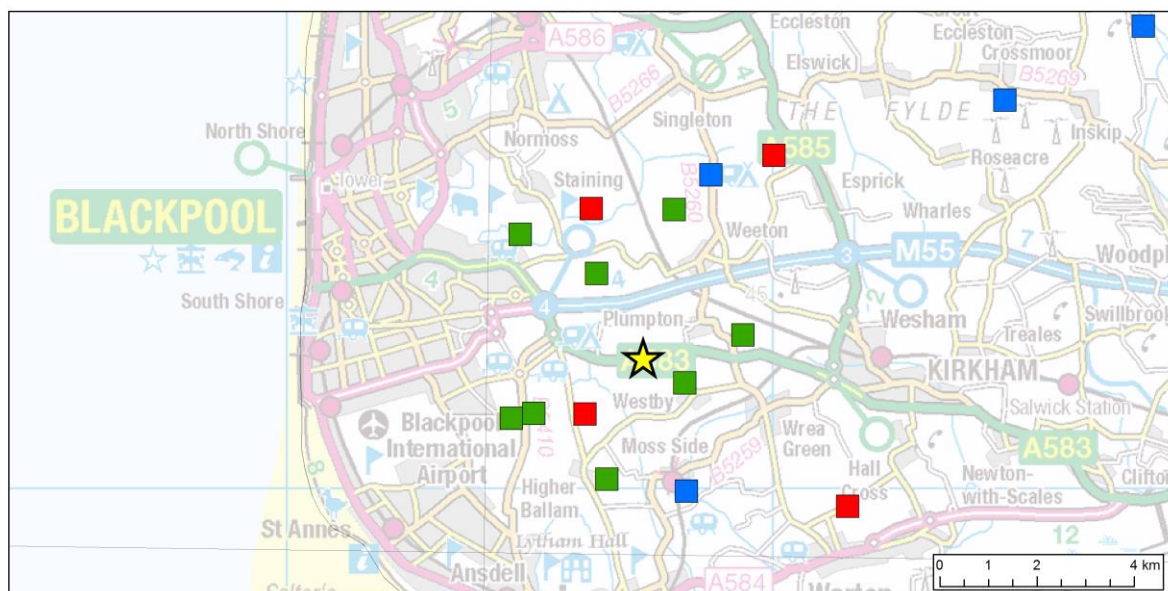
Figure 2.2. Surface stations deployed by Cuadrilla Resources Ltd (green squares), the British Geological Survey (red squares) and the University of Liverpool (blue squares).

Events were detected in near real-time using the Carltrig STA/LTA algorithm (Johnson et al., 1995). However, this only resulted in 57 detections for PNR-1z and 125 for PNR-2. For PNR-1z. 22 of these had magnitudes greater than 0.0 ML, the amber TLS threshold, and 7 had magnitudes greater than the TLS limit of 0.5 ML. Baptie and Luckett (2019) used cross-correlation template-matching (e.g. Shelly et al, 2013) to find an additional 115 events, all with magnitudes of less than 0.0 ML during operations at PNR-1z. However, for this study we simply use the origin times of the events in downhole catalogue to extract the same events from the continuous waveform data recorded at surface stations, incrementally reducing the lower magnitude cut-off until the observed signal cannot be discriminated from the background noise. This approach yielded a total of 188 events from the downhole catalogue from PNR-1z and 260 events from PNR-2 that could be observed on a minimum of three surface stations.

2.1   EVENT LOCATIONS

Locations for all events are shown in Figure 2.3. Events are coloured by time and move from west to east corresponding to different stages of hydraulic fracturing in PNR-1z. The locations of the events closely correspond to the positions of the sleeves that were hydraulically fractured (coloured squares in Figure 2.3). Clark et al (2019) interpret the seismicity as a result of the intersection of the hydraulic fracturing with a pre-existing network of fractures or faults that became seismically active. This may result in the rather diffuse distribution of the seismicity. Event locations also move from west to east during operations in PNR-2 (Figure 2.3c), however, unlike

the seismicity during operations in PNR-1Z, the seismicity in PNR-2 shows strong alignment along a number of distinct NNW-SSE planes with lengths of up to 750 m. This spatial alignment is more typical of hydraulic fracturing, with fracture networks opening perpendicular to the minimum compressive stress. This difference in the spatial distribution of event locations between PNR-1z and PNR-2 may also result from differences in lithology between the Upper and Lower Bowland Shale (J. Verdon, pers. comm.), with PNR-1z in the Lower and PNR-2 in the Upper. This difference in the well depths is reflected in the event depths. These are around 2280 m for PNR-1z (Figure 2.3b), but decrease slightly from around 2300 m at the toe of the well to approximately 2250 m closer to the heel. The depth cross-section (Figure 2.3d) shows that the depths of the events at PNR-2 are tightly constrained from around 1980 m to 2220 m.
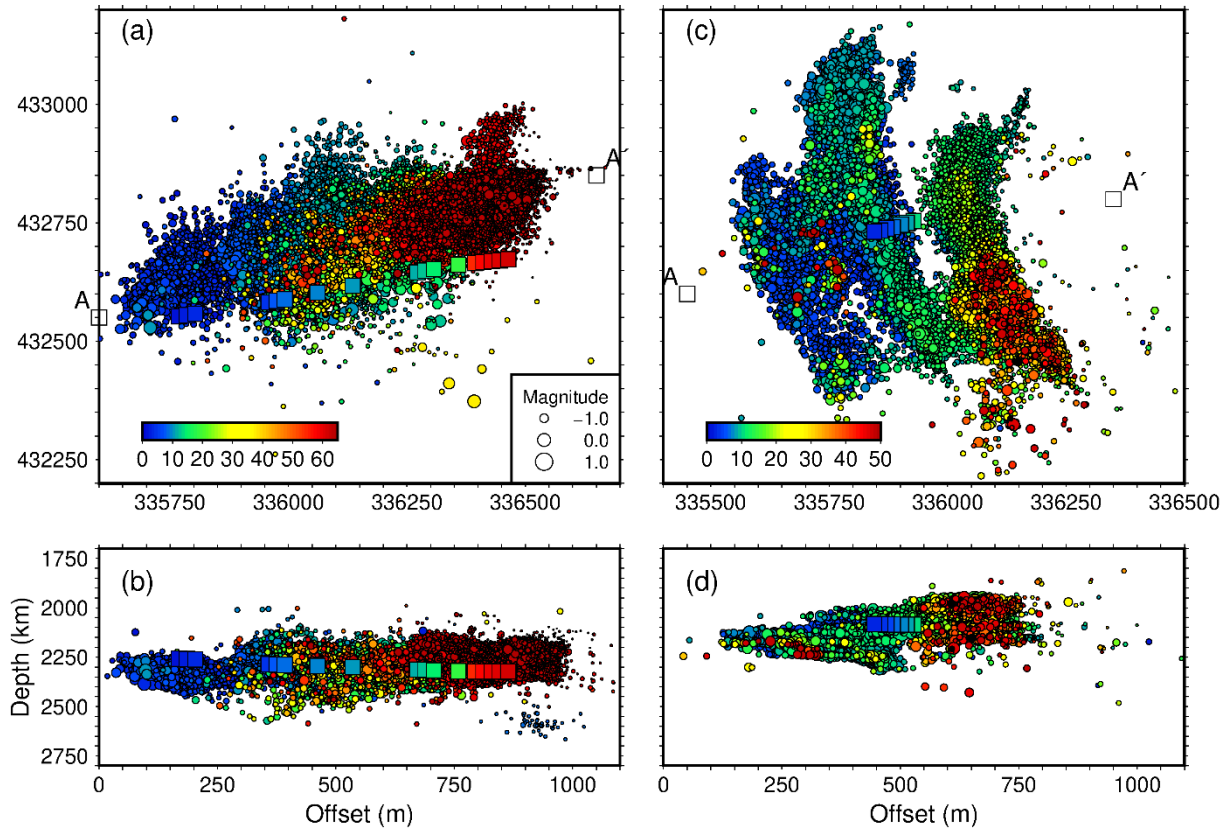
Figure 2.3. Maps of all events in the microseismic catalogue recorded during operations in PNR-1Z (a) and PNR-2 (c). Events are coloured by time in days from the start of operations and scaled by magnitude. The coloured squares in (a) show the locations of the sleeves that were hydraulically fractured in PNR-1Z. The squares are coloured using the same colour scale as the events. Axes show British National Grid Eastings and Northings. (b) and (d) show depth cross-section showing event depths along the profile A-A´.

2.2 FREQUENCY MAGNITUDE DISTRIBUTION

The relationship between the magnitude and number of earthquakes in a given region and time period generally takes an exponential form that is referred to as the Gutenberg-Richter law (Gutenberg and Richter, 1954), and is commonly expressed as

$$\log_{10} N = a - bM \qquad (2.1)$$

where N is the number of earthquakes above a given magnitude M. The constant a is a function of the total number of earthquakes in the sample and is known as the earthquake rate. This is often normalised over a period of time, such as a year. The constant b gives the proportion of large events to small ones, and is commonly referred to as the b-value. In general, b-values are close to unity for tectonic earthquakes. This means that for each unit increase in magnitude, the number of earthquakes reduces tenfold. However, higher b-values have often been observed for induced seismicity (e.g. Bachmann et al, 2011).

Figure 2.4 shows the frequency magnitude distributions determined from both the surface and downhole catalogues of events from PNR-1z and PNR-2, together with the maximum likelihood estimates of the *b*-value and activity rate for calculated completeness magnitudes of -1.0 and -0.5 for the downhole and surface catalogues respectively. The completeness magnitude, Mc, is defined as the lowest magnitude at which (approximately) 100% of the earthquakes in a space time volume are detected (Rydelek and Sacks, 1989). We use bootstrap resampling with 4000 replicates of the catalogues to estimate non-parametric confidence intervals for the *b*-value and activity rate. The error bars for the cumulative data show 95% confidence limits determined from a χ^2 distribution with the number of degrees of freedom specified by the cumulative number of events in each
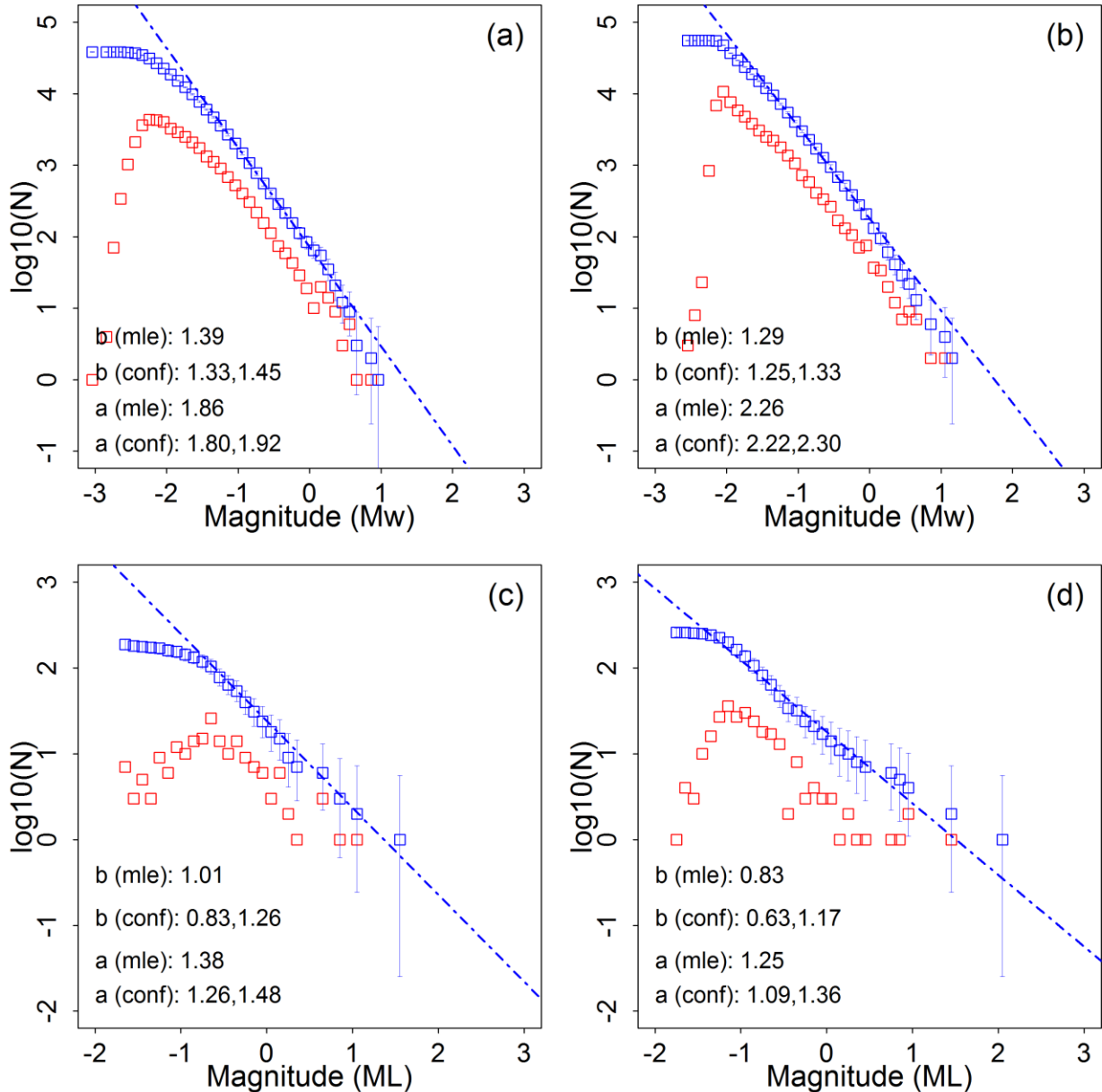
Figure 2.4. Frequency magnitude distributions for: (a) PNR-1z downhole catalogue; (b) PNR-2 downhole catalogue; (c) PNR-1z surface catalogue; and (d) PNR-2 surface catalogue. Red and blue dashed squares show incremental and cumulative data. Error bars show 95% confidence limits determined from a χ^2 distribution with the number of degrees of freedom specified by the cumulative number of events. The blue dashed lines show the maximum likelihood estimates of the b-value and activity rate for a completeness magnitude of -1.0 for the downhole catalogues and -0.5 for the surface catalogues. Confidence limits are from bootstrap resampling. The magnitude 2.9 ML event on 26 August 2019 was not recorded by the downhole array so is not included in the catalogue of matching events.

magnitude bin. The downhole data show moment magnitudes (Mw) and the surface catalogues show local magnitudes (ML). The b-values for the downhole catalogues are larger than those commonly observed for tectonic seismicity, with values of approximately 1.4 and 1.3 for the 2018 and 2019 seismicity respectively. Such values have important implications for hazard assessments, since the b-value is commonly used to estimate the probability of larger seismic events, and a high factor decreases the chance of larger events relative to natural seismicity. However, at higher magnitudes, it is clear that there is an apparent roll-off in the observed frequency magnitude data from the downhole catalogues (Figure 2.4 (a) and (b)). This could be a result of a number of factors, including the limited dynamic range and frequency response of the downhole instrumentation, or possibly the parameterisation and method used to determine moment magnitudes. The effect of the known gaps in the downhole catalogues on the overall frequency magnitude distribution is difficult to quantify.

3 Magnitude Estimation

Earthquake magnitude is a measure of the amount of energy released during an earthquake. A number of different magnitude scales have been developed generally based on the amplitude of different parts of the observed record of ground motion, often in a particular frequency range, and with specific corrections for distance.

3.1   LOCAL MAGNITUDE

The first magnitude scale was developed by Richter (1935) using observations of earthquakes in Southern California and although the scale is only strictly applicable there, it has been used all around the world and is commonly referred to as Local Magnitude, ML. Richter (1935) defined this as

$$M_L = \log_{10}\left(\frac{A}{A_0}\right) \tag{3.1}$$

where A is the largest zero-to-peak maximum deflection, in millimetres registered by the earthquake on a Wood-Anderson seismograph, and A_0 is the deflection produced by a "standard" magnitude zero earthquake at the same distance. The A_0 factor allows observed amplitudes to account for attenuation between the seismograph and the epicentre of the earthquake. The scale is logarithmic so that each whole number increase in magnitude represents a tenfold increase in measured amplitude and about 32 times the energy released.

Bakun and Joyner (1984) suggested replacing the tabulated values for the A_0 factor by an attenuation curve described in terms of distance and log of distance and Hutton and Boore (1987) used data from southern California to determine such a distance correction curve, defining local magnitude as

$$M_L = \log_{10}(a) + 1.11\log_{10}(r) + 0.00189r - 2.09 \tag{3.2}$$

where a is the displacement amplitude in nanometres and r is the hypocentral distance in kilometres. Booth (2007) showed that these parameters may also be considered appropriate in the UK and Ottemöller and Sargeant (2013) used UK data to find the relation

$$M_L = \log_{10}(a) + 1.06\log_{10}(r) + 0.00182r - 1.98 \tag{3.3}$$

Although Richter's original calculations were derived from ground motions measured at a range of distances, this did not include any measurements made within a few kilometres of the earthquake source. Butcher et al. (2016) show that amplitude measurements from epicentral distances of less than 15-20 km considerably overestimate event magnitudes compared to more distant observations. Similarly, magnitudes calculated for earthquakes induced by hydraulic fracturing at Preese Hall, Lancashire, using ground motions recorded on seismometers distances

of a few kilometres away were unrealistically high (Clarke et al., 2014). Luckett et al. (2019) incorporate a correction for near source observations to address this issue, finding

$$M_L = \log_{10}(a) + 1.11\log_{10}(r) + 0.00189r - 1.16e^{-0.2r} - 2.09 \tag{3.4}$$

Local magnitudes for events recorded on surface stations were determined from the largest zero-to-peak displacement in nanometres on horizontal component waveforms with a signal-to-noise ratio of greater than 2 that were high-pass filtered at 1.25 Hz (Figure 3.1). Magnitudes were then calculated using the UK local magnitude (ML) scale of Luckett et al. (2019), incorporating a correction for near source observations. Hypocentral distances were calculated using the downhole catalogue locations for common events as these were considered to be more reliable. This is clear from a comparison of the hypocentres in each catalogue, with the surface locations showing considerably more scatter. A minimum of four amplitudes were measured for each event, although for most events, a larger subset of the recording stations was used. The event magnitude is taken as the mean of the magnitudes measured at each station.
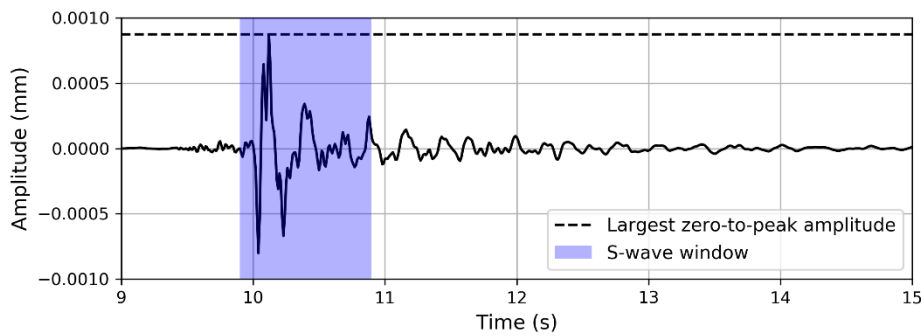
Figure 3.1. Example earthquake recording captured on station AQ04 on the 29th October 2018. Local magnitudes (ML) are measured from the largest zero-to-peak amplitude (black dashed line) on the horizontal component; moment magnitudes (Mw) are calculated using the S-wave phase (shaded area) in the frequency domain.

3.2   MOMENT MAGNITUDE

Moment magnitude, Mw, is generally considered a more reliable measure of earthquake size, and is based on seismic moment, defined as

$$M_0 = \mu A D \tag{3.5}$$

where μ is the modulus of rigidity of the faulted rock, A is the area of the rupture and D is the amount of slip on the rupture. Typical values for μ are 32 GPa in the crust and 75 GPa in the mantle. Moment is therefore related to both the area of the rupture and the displacement on the rupture. Following Hanks and Kanamori (1979) seismic moment is related to the moment magnitude, Mw, by

$$M_W = \frac{2}{3}\log_{10} M_0 - 6.06 \tag{3.6}$$

with M_0 (in units of Nm) usually estimated directly from recordings of earthquake ground motions. The amplitude spectrum of the ground displacement at some distance from an earthquake has a constant value at low frequencies and is inversely proportional to frequency (squared) at higher frequencies (Aki and Richards, 2002). Brune (1970) gave the far-field displacement spectrum as

$$\Omega(f) = \frac{\Omega_0}{1 + \left(\frac{f}{f_c}\right)^2} \tag{3.7}$$

where Ω_0 is the low frequency level of the spectrum and f_c is the corner frequency that controls the decay of the spectrum with frequency. Ω_0 is a function of the seismic moment, the velocity and density of the rock at the earthquake source and the distance from the source. Corner frequency is proportional to both the seismic moment and the stress drop.

We follow the frequency domain approach of Stork et al. (2014) and Havskov and Ottemoller (2003) to estimate M_0 and calculate Mw. After removing the instrument response and applying a 20% cosine taper, a 1 second window after the first S-wave arrival is transformed into the frequency domain using the multi-tapering techniques developed by Prieto et al. (2009). Noise spectra are subtracted from the resulting source spectra. These are modeled using a Brune (1970) model,

$$\Omega(f) = \frac{\Omega_0 e^{-\left(\frac{\pi f t}{Q}\right)}}{[1 + (f/f_c)^2]}, \tag{3.8}$$

where Ω_0 is the low frequency plateau, f is frequency, f_c is the corner frequency, t is the travel time between source and receiver and Q is the quality factor. The model includes a travel path correction for anelastic attenuation (Q) which is assumed to be frequency independent. Figure 3.2 shows and example of an observed and modelled amplitude spectrum.
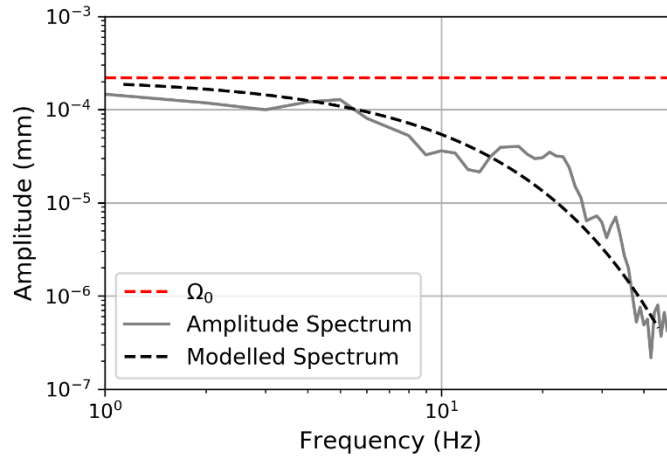
Figure 3.2. Amplitude spectrum (grey line) from the windowed S-wave arrival (see Figure 3.1.). Ω_0 (red dashed line) is estimated using a Brune source model (black dashed line), which also provides measurements of both Q and f_c.

In the frequency domain the seismic moment (M_0) of a recorded seismic signal can be expressed as

$$M_0 = \frac{4\pi\rho v^3 d\Omega_0}{FR}, \tag{3.9}$$

where d is the hypocentral distance, v is S-wave velocity at the source, ρ is the rock density at the source, F is the free surface amplification factor which is assigned a value of 2, and R is a term relating to the radiation pattern. The S-wave is used to measure Mw, and therefore an average radiation pattern correction of 0.60 is applied (Boore and Boatwright, 1984). Velocity and density in this calculation are those at the source location. We use velocities taken from the Cuadrilla velocity model of 2.7 km/s and v=3.0 km/s for PNR-1z and PNR-2, respectively. We use a density of 2.5 g/cm^3 for both PNR-1z and PNR-2. As stated previously, because no information was available on how the magnitudes in the downhole catalogues were determined, we are unable to say if our choice of parameters is the same, or if these parameters may have changed either between operations or during operations.

The event Mw is the mean of the magnitudes calculated on both horizontal components on each station. Mw is primarily controlled by the low frequency plateau value, which is relatively

unaffected by attenuation along the travel path (Ross et al., 2016). The parameterization of Equation 3.9 does, however, have a significant effect on the estimate, with Mw sensitive to the choice of v and ρ, which are both difficult to constrain as they represent values at the source location.

3.3 RELATIONSHIP BETWEEN MOMENT AND LOCAL MAGNITUDES

A divergence between scales is commonly observed at low magnitudes, with Mw becoming progressively larger than ML as magnitudes decrease. ML-Mw relationships are typically empirical scales derived from existing earthquake catalogues. Those that contain observations with $M_L > 3$ commonly observe a relationship close to 1:1 between ML and Mw (Fäh et al., 2011; Ottemöller and Sargeant, 2013), while those including M < 3 typically use either a quadratic term to fit the data (Grünthal et al., 2009; Edwards et al., 2010) or a different scaling relationship (Munafò et al., 2016). A relationship between ML and Mw was derived using data recorded on surface sensors during operations in PNR-1z by the consultants Q-con and is published in the hydraulic fracture plan for PNR-2 (Cuadrilla, 2019). This relationship is derived from Munafò et al. (2016) and shows a linear relationship between ML and Mw in the magnitude range -1.0 – 1.5 ML. In our subsequent analysis we use this scale as a reference with which to compare the surface and downhole magnitudes.

Calculating theoretical spectra for a range of different earthquake magnitudes gives a family of self-similar spectra that are scaled by magnitude and whose corner frequencies increase as magnitude decreases (Figure 3.3). As a result, smaller earthquakes not only have less energy than larger earthquakes, but their seismic waves contain (relatively) higher frequency content. High frequency energy more rapidly decays with distance than low frequency energy. This imposes a maximum frequency limit on the source spectra of very small events. This limit is a function of the intrinsic attenuation of the material through which the seismic energy has travelled (Deichmann, 2017; Staudenmaier et al., 2018).
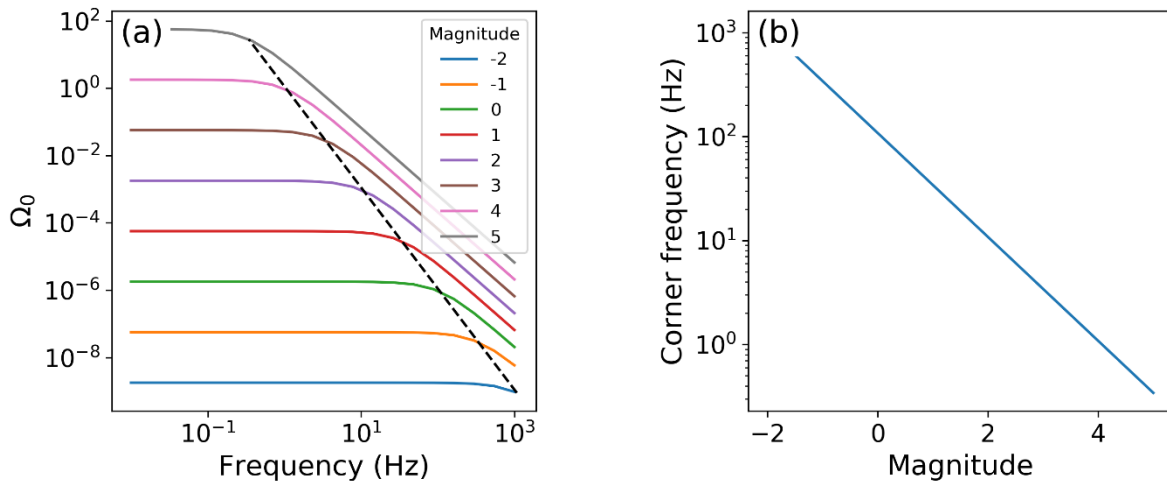
Figure 3.3. (a) Theoretical displacement spectra for different earthquake magnitudes using the Brune (1970) model. Spectra are calculated for a stress drop of 1 MPa. The dashed line connects the corner frequency for each spectrum. (b) shows corner frequencies for different magnitudes.

Although ML and Mw are theoretically equivalent in a perfectly elastic medium (Deichmann, 2006), the introduction of this high-frequency limit causes a breakdown in the relationship between corner frequency and moment, producing the relationship Mw = 2/3ML + C (Deichmann, 2017). An example of this effect is shown in Figure 3.4., where the observed spectra (Figure 3.4a) show a roughly constant corner frequency with magnitude, in contrast to the modelled spectra, in which corner frequencies of the smallest events continue increasing (Figure 3.4b). A constant fc can explain the breakdown in linearity between the two magnitude scales, as the loss of high frequency

energy will act to reduce the maximum amplitude in the time-domain (Butcher et. al., 2020). Magnitudes calculated using ML will therefore be smaller than Mw, which are estimated using the low frequency plateau, Ω_0, and unaffected by the introduction of a near constant f_c. In addition, larger events may contain significant amounts of energy below the 15 Hz corner high frequency of the downhole geophones that might lead to lower recorded amplitudes for these events and corresponding underestimates of Mw.
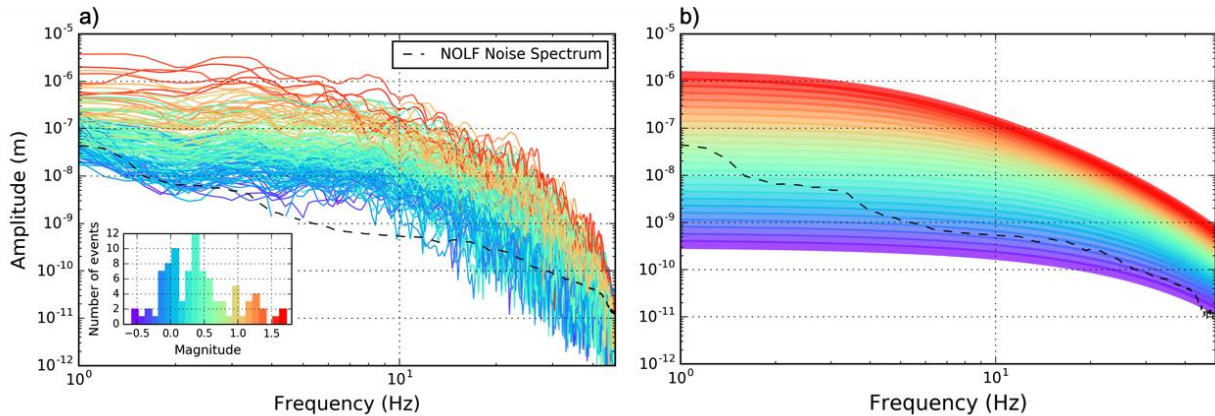
Figure 3.4. (a) Source frequency spectra for a cluster of small mining-induced events at New Ollerton, UK. Colours indicate the magnitude of the event, as shown by the histogram inset. (b) Brune modelled source spectrum and using a 1:1 scaling relationship between M_L and M_W. While in general there is agreement between the modelled and observed data at larger magnitudes, there is a clear difference compared with the observed data at lower magnitudes: the smallest events are depleted in high frequency amplitude relative to the theoretical spectra; the corner frequency no longer increases with decreasing magnitude.

4 Results

Magnitude estimates for PNR-1z and PNR-2 (Figure 4.1) are plotted alongside relevant ML-Mw relationships derived for small earthquakes in Switzerland (Goertz-Allmann et al, 2011), the northern Apennines, Italy (Munafò et al., 2016), Groningen, the Netherlands (Dost et al, 2018) and New Ollerton, UK (Butcher et al, 2020). Also shown is the relationship between ML and Mw developed by Q-con (Cuadrilla, 2019) using data from PNR-1z. Surface magnitudes have been recalculated by the authors using event locations derived from the downhole array, while downhole estimates of both ML and Mw have been provided by the operator. Details of the parameters used to calculate the downhole estimates are limited (e.g. source velocity and density), though PNR-1z downhole ML estimates appear to be based on the scale of Luckett et al. (2019).

Considering the magnitude range of the PNR-1z datasets, the downhole observations extend much lower than the surface dataset, while at the upper end downhole magnitudes are less than those calculated from the surface data. The lower detectability limit is primarily due to the closer proximity of the downhole instruments to the source as well as the lower noise levels. This proximity is however problematic at higher magnitudes, where the downhole geophones become saturated imposing an upper limit on ML. In addition, estimates of Mw are also reduced at higher magnitudes as the corner frequency approaches the sensitivity range of the geophones, which for PNR-1z was 15Hz. These factors have little effect on the surface measurements, which were recorded using broader frequency range instruments located at greater hypocentral distances.

Combining the surface and downhole datasets overcomes both the detectability limitations of the surface data and the saturation issues with the downhole observations. For both PNR-1z and PNR-2 there is a clear offset between these datasets when comparing overlapping observations in Figure 4.1. The differences between ML and Mw in the downhole catalogues are less than those in both

the surface catalogues and in the relationships developed for different regions. In contrast, magnitude estimates calculated from surface receivers show reasonable agreement with published ML-Mw relationships. The magnitude estimates from surface data also show reasonable agreement with the Q-con relationship at higher magnitudes, but begin to diverge at lower magnitudes, particularly for PNR-1z. This may be because we have estimated both moment and local magnitudes for much smaller events. The observed offsets imply that either ML has been systematically overestimated and/ or Mw has been underestimated in the downhole catalogue. The PNR-2 dataset has fewer observations with a sufficient SNR to compute a surface Mw, with a lower estimation limit of approximately Mw=0.5 which is slightly higher than PNR-1z. These events are also consistent with the relationship developed by Q-con and also comparable to the relationship of the surface PNR-1z.
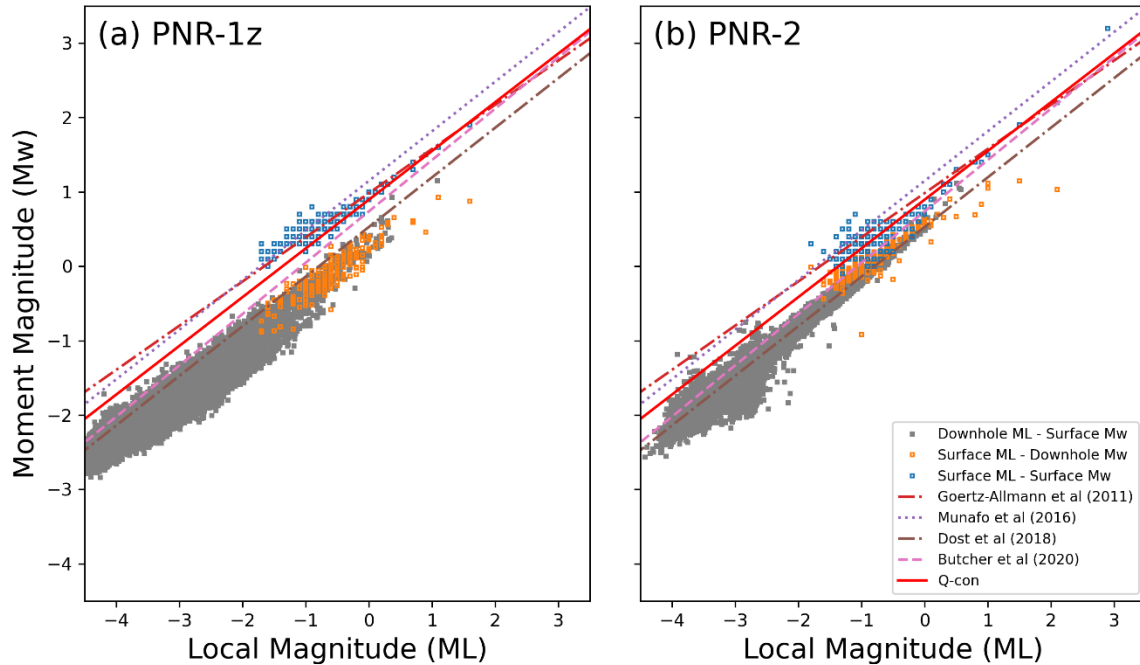
Figure 4.1. Magnitude data from PNR-1z (a) and PNR-2 (b). Grey squares show local and moment magnitudes from the downhole catalogues. Blue squares show local and moment magnitudes from the surface catalogue. Orange squares show surface local magnitudes and downhole moment magnitudes for common events in both catalogues. Surface estimates appear consistent with other published relationships, including the Q-con relationship, while the downhole catalogues are significantly offset.

To consider the cause of these discrepancies in both the PNR-1z and PNR-2 downhole datasets in more detail, we compare the differences in magnitude for common events in both the surface and downhole catalogues from PNR-1z and PNR-2. Figure 4.2 shows the difference between surface magnitude measurements and downhole magnitudes as a function of surface magnitude for both Mw and ML. For PNR-1z, there is a systematic offset between the surface and downhole Mw of approximately 0.6 (Figure 4.2a), which follows the offset observed in Figure 4.1. This suggests that the downhole Mw values have been systematically underestimated across a wide range of magnitudes. For PNR-2, the difference between surface and downhole Mw (Figure 4.2b) is less than for PNR-1z. It is difficult to identify a clear systematic trend due to scatter in the data, but the difference between surface and downhole Mw may increase as with magnitude.

The differences between the surface and downhole ML estimates for PNR-1z (Figure 4.2c) show considerable scatter, but suggest that the surface and downhole measurements are similar until magnitudes of around 0.2 ML. At higher magnitudes the surface ML estimates are increasingly greater than the downhole estimates, possibly as a result of the limitations of the downhole data

acquisition. For PNR-2 (Figure 4.2d), the differences between the surface and downhole ML clearly increase with increasing magnitude.
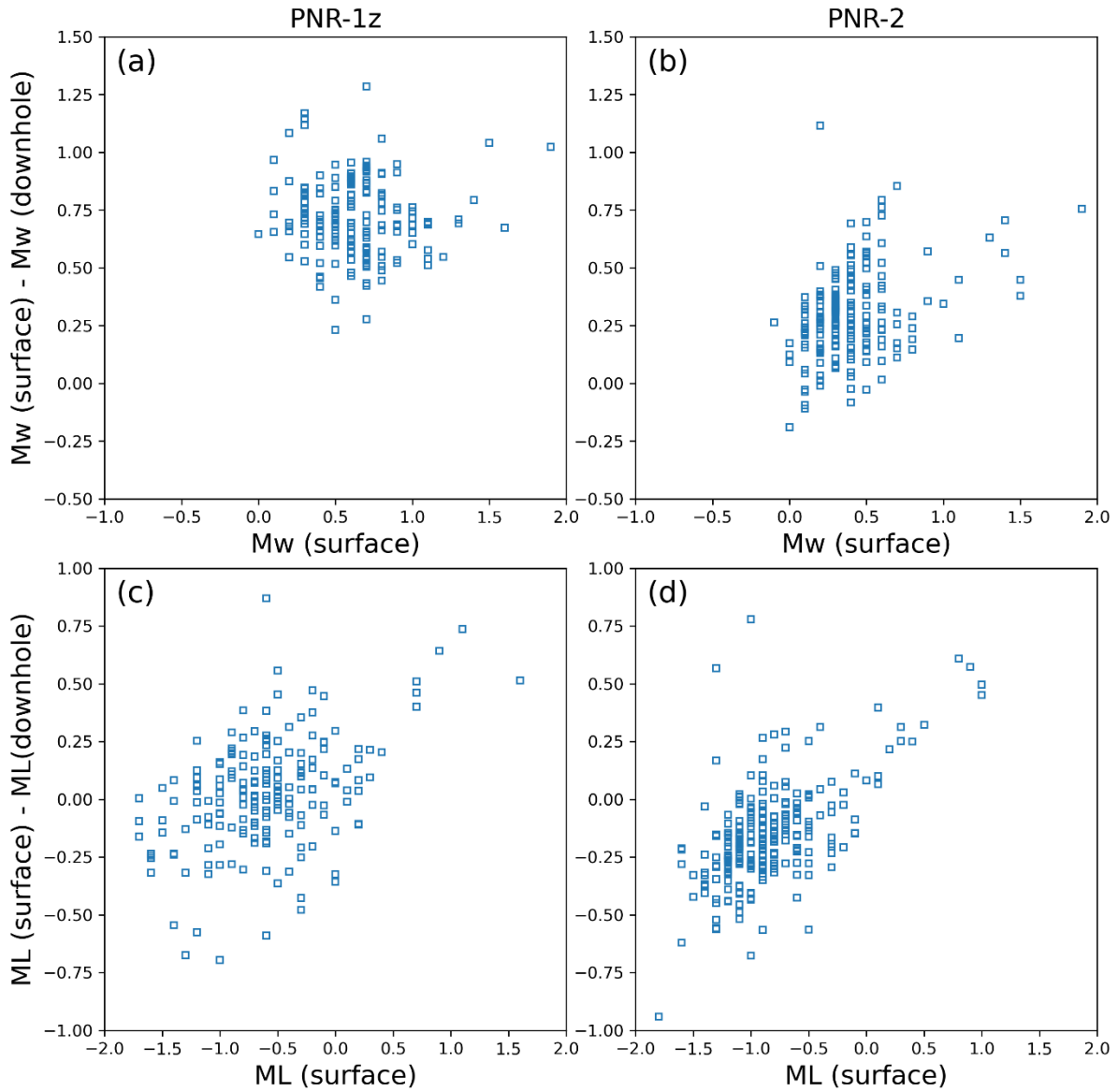
Figure 4.2. Difference between surface and downhole magnitude estimates for common events in both the surface and downhole catalogues. (a) and (b) show surface and downhole moment magnitudes from PNR-1z and PNR-2, respectively. (c) and (d) show surface and downhole local magnitudes from PNR-1z and PNR-2, respectively.

4.1 MAGNITUDE ADJUSTMENT USING SURFACE ML

One approach to correcting the moment magnitude estimates in the downhole catalogues is to reference them to a common relationship between surface moment magnitude and surface local magnitude. This may be appropriate where direct estimates of surface moment magnitude are not available or where there are a limited number of surface observations, making it difficult to constrain the relationship between ML and Mw. In this case we use the relationship derived by Q-con using measurements of both moment and local magnitude from data recorded on surface sensors during operations in PNR-1z and intended for use during operations in PNR-2,

$$M_w(predicted) = + 0.655 \, M_L(surface) + 0.897 \tag{4.1}$$

Figure 4.3 shows Mw from the downhole catalogue as a function of ML from the surface recordings for all common events for (a) PNR-1z and (b) PNR-2. Also shown is the best-fitting straight line fit to the data determined using orthogonal distance regression (ODR) (e.g. Castellaro et al, 2006) and the relationship between surface ML and Mw measurements determined by Q-con (Cuadrilla, 2019). Our regression is derived using only downhole moment magnitudes that are less than 0.5 Mw to avoid using magnitude estimates for larger events that are clearly affected by limitations of the data acquisition. It is clear that there are considerable differences between the ML-Mw relationships from PNR-1z and PNR-2 and also with the Q-con relationship. Given that the surface ML estimates can be considered as stable and constant between all three relationships, as shown in Figure 4.1 the downhole Mw estimates are significantly lower than either those measured from the surface data or those estimated using an ML-Mw relationship. As discussed previously, this may result from differences in the parameters used for fitting the source spectra and also from differences in the frequency response and dynamic range of the downhole geophones that cause the amplitude of signals to be systematically underestimated. The underestimation of Mw in the PNR-1z catalogue is greater than in the PNR-2 catalogue, despite similar instrumentation.
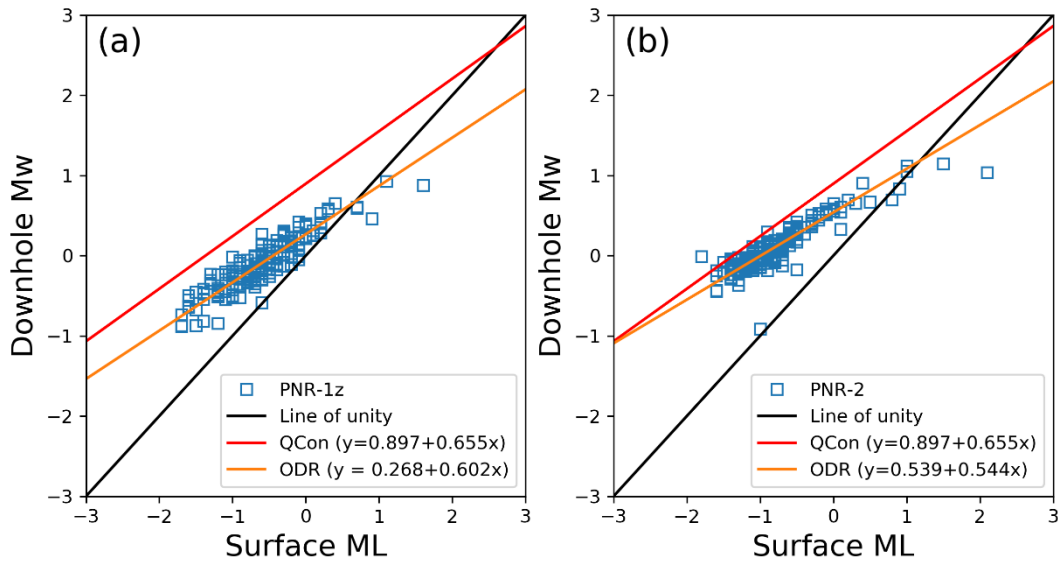
Figure 4.3. Mw values from the downhole catalogue plotted against ML estimates for common events in the surface catalogue for (a) PNR-1z and (b) PNR-2. The black line shows the line of unity and the red line shows the ML-MW relationship derived from surface data by Q-con. The orange line shows the best fit to the data determined using orthogonal distance regression. The magnitude 2.9 ML event on 26 August 2019 was not recorded by the downhole array so is not included in the catalogue of matching events.

The ML-Mw relationship derived for the PNR-1z data for moment magnitudes of less than 0.5 Mw using orthogonal distance regression is

$$M_w \,(downhole) = 0.602 \, M_L \,(surface) + 0.268 \qquad (4.2)$$

The ML-Mw relationship derived for PNR-2 for moment magnitudes of less than 0.5 Mw is

$$M_w \,(downhole) = 0.544 \, M_L \,(surface) + 0.539 \qquad (4.3)$$

For PNR-1z, combining equations (4.1) and (4.2) allows us to convert the downhole moment magnitudes to a predicted surface moment magnitude using

$$M_w \,(predicted) = 1.088 \, M_w \,(downhole) + 0.605 \qquad (4.4)$$

This suggests that there is almost a constant offset of approximately 0.6 Mw between the surface and downhole moment magnitude estimates for all magnitudes.

Similarly, for PNR-2, by combining equations (4.1) and (4.3), the downhole moment magnitudes can be converted to a predicted surface moment magnitude using

$$M_w\,(predicted) = 1.204\,M_w\,(downhole) + 0.248 \qquad (4.5)$$

This suggests that the relationship between surface and downhole moment magnitude is more strongly dependent on magnitude than for PNR-1z.

We apply equations (4.4) and (4.5) to all events in the respective downhole catalogues for which we do not also have a measure of surface local magnitude. For those events for which we have a surface local magnitude, we use equation (4.1) to predict surface moment magnitude directly, ensuring that we have a more reliable estimate of moment magnitude for the larger events. This approach gives us revised catalogues for PNR-1z and PNR-2 that contain predicted moment magnitudes for all events.

We independently check the revised downhole moment magnitude by comparing them with the measured surface moment magnitudes for common events in the surface and downhole catalogues. Figure 4.4 shows revised downhole moment magnitude plotted against moment magnitudes determined from the surface data for PNR-1z (a) and PNR-2 (b). While there is scatter in the results, there is reasonable agreement between the two independent data sets.
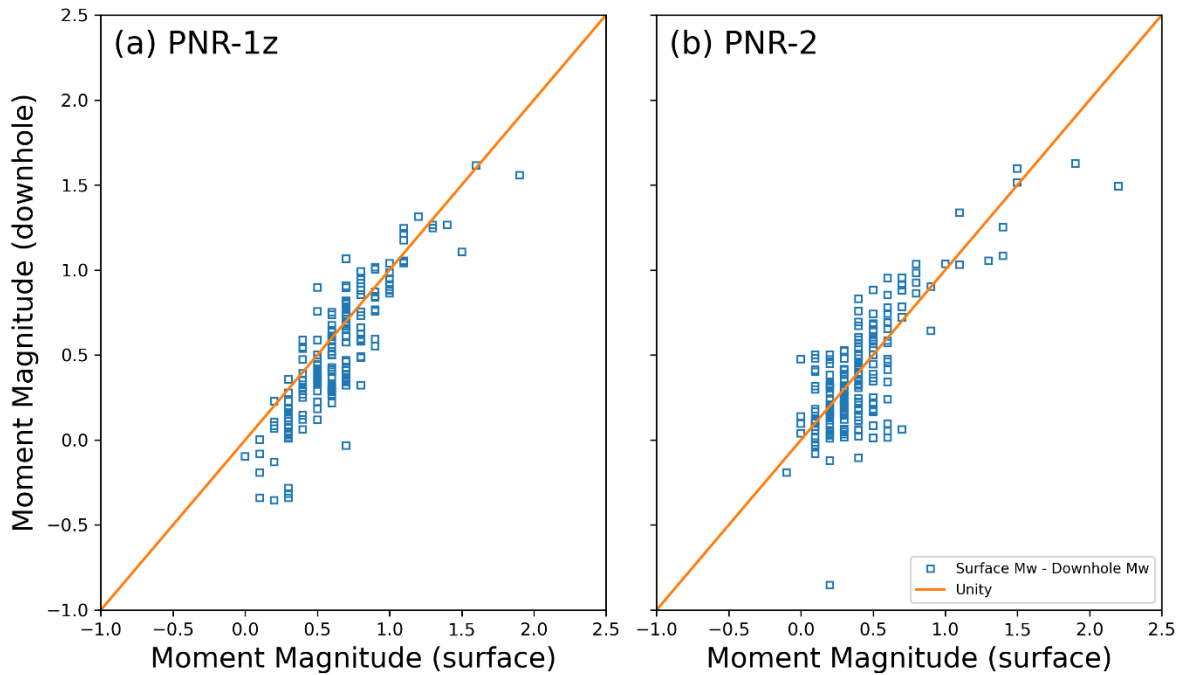
Figure 4.4. Revised downhole moment magnitudes plotted against moment magnitudes determined from the surface data for PNR-1z (a) and PNR-2 (b). The downhole moment magnitudes are corrected using equations (4.4) and (4.5) for PNR-1z (a) and PNR-2 (b), respectively. The orange line shows the line of unity.

Frequency-magnitude distributions for these revised catalogues are shown in Figure 4.5. Confidence intervals for the *b*-values and activity rates are estimated using bootstrap resampling and the error bars for the cumulative data show 95% confidence limits determined from a χ^2 distribution. The previous truncation at higher magnitudes is no longer as apparent. The near linear shift in the magnitudes of PNR-1z catalogue results in a significant increase in activity rate from 1.86 to 2.62, while the *b*-value reduces slightly from 1.39 to 1.27, still relatively high. However, for PNR-2, the gradient of the magnitude conversion relationship means that while activity rate increases slightly from 2.26 to 2.51, the *b*-value shows a significant reduction from 1.29 to 1.06, reflecting a relative increase in the number of larger events to smaller ones. There is also now quite a difference in *b*-value between PNR-1z and PNR-2, which may be related to the different

behaviour of the seismicity, with post-operations event rates in PNR-2 decaying more slowly than for PNR-1z and many more trailing events with larger magnitudes.
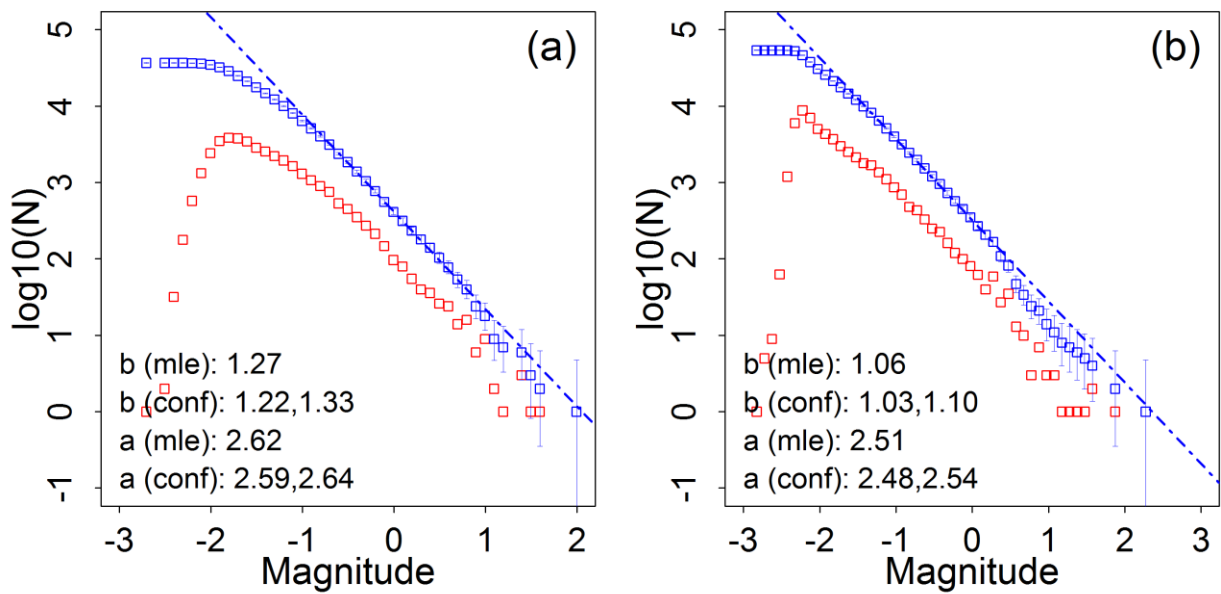
Figure 4.5. Revised frequency magnitude distributions for the downhole catalogues of PNR-1z (a) and PNR-2 (b). Original moment magnitudes are either converted to an equivalent surface moment magnitude using equations (4.4) and (4.5), or for common events, are replaced by an equivalent surface moment magnitude calculated from surface local magnitude using the Q-con relationship.

To examine the scaling between ML and Mw in more detail, we compare the difference between downhole Mw and surface ML as a function of surface ML (Figure 4.6) after correcting the original downhole moment magnitudes to an equivalent surface moment magnitude using equations 4.3 and 4.4. This shows that the difference between ML and Mw increases as magnitude decreases. Given that for ML between 3 and 6 the proportionality coefficient between ML and Mw is usually close to 1 (Bakun, 1984; Hanks & Boore, 1984), this result provides further evidence for differences in scaling between ML and Mw between small earthquakes and larger ones (e.g. Staudenmaier et al, 2018).
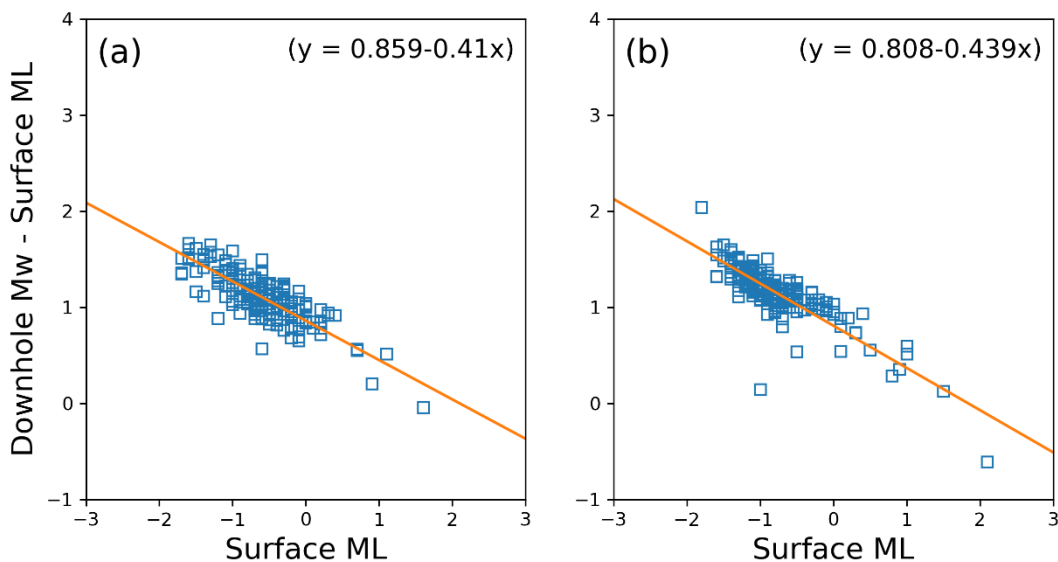
Figure 4.6. Observed scaling between corrected downhole moment magnitudes and surface local magnitudes for common events in each catalogue.

4.2   MAGNITUDE ADJUSTMENT USING SURFACE MW

An alternative approach to correcting the downhole moment magnitudes is to use a direct relationship between surface and downhole moment magnitudes. This obviously requires surface moment magnitudes to constrain this relationship. Figure 4.7 shows Mw measured from surface recordings as a function of Mw from the downhole catalogue for all common events for (a) PNR-1z and (b) PNR-2. Orange lines show the best-fitting straight line fit to the data determined using orthogonal distance regression.
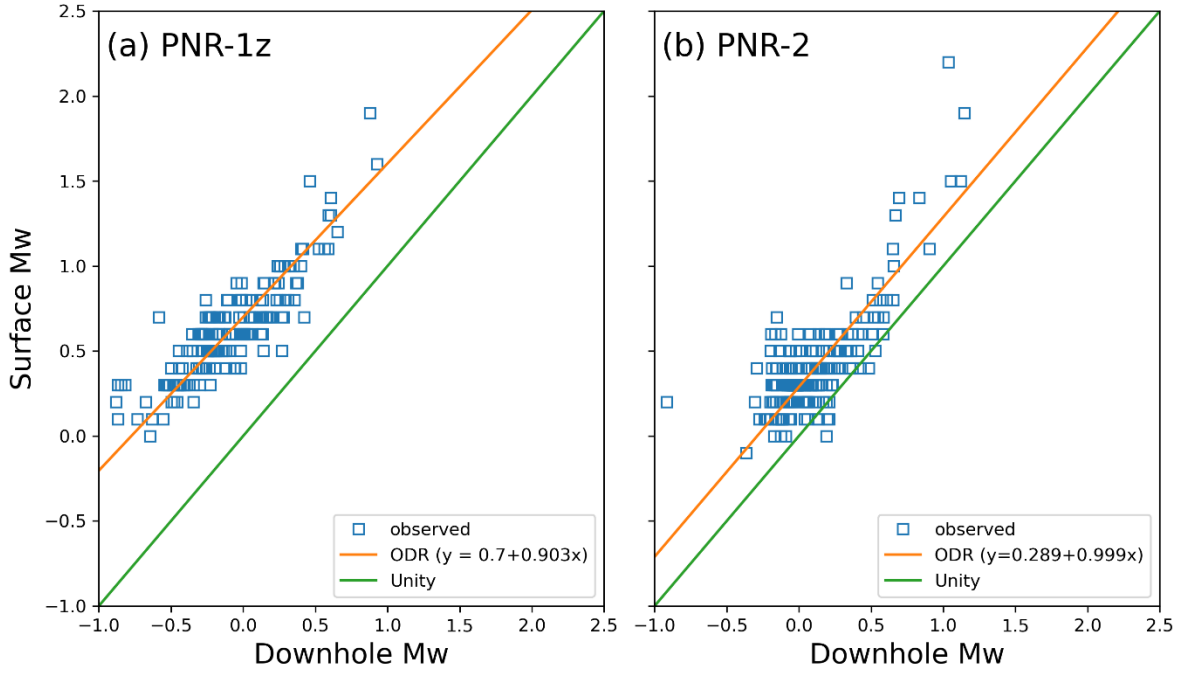
**Figure 4.7. Mw values from the downhole catalogue plotted against Mw for common events in the surface catalogue for (a) PNR-1z and (b) PNR-2. The green line shows the line of unity. The orange line shows the best fit to the data determined using orthogonal distance regression. The magnitude 2.9 ML event on 26 August 2019 was not recorded by the downhole array so is not included in the catalogue of matching events.**

The regression is derived using only downhole moment magnitudes that are less than 1.0 Mw. The data from both PNR-1z and PNR-2 show a similar trend to the line of unity, but the PNR-1z data have a significantly larger offset. The PNR-2 data show more scatter then PNR-1z.

The relationship between surface and downhole moment magnitude for PNR-1z for moment magnitudes of less than 1.0 Mw is

$$M_w(surface) = 0.903\, M_w(downhole) + 0.7 \qquad (4.6)$$

The relationship between surface and downhole moment magnitude for PNR-2 for moment magnitudes of less than 1.0 Mw is

$$M_w(surface) = 0.999\, M_w(downhole) + 0.289 \qquad (4.7)$$

Equations (4.6) and (4.7) can be compared directly with equations (4.4) and (4.5). For PNR-1z, equations (4.4) and (4.6) are comparable. For PNR-2, equations (4.5) and (4.7) show more difference, with equation (4.4) showing greater dependence on magnitude.

We apply equations (4.6) and (4.7) to all events in the respective downhole catalogues for which we do not also have a measure of surface moment magnitude. For those events that do have a surface local magnitude, we replace the downhole moment magnitude with the surface estimate. Again, this approach gives us revised catalogues for PNR-1z and PNR-2 that contain predicted moment magnitudes for all events.

Frequency-magnitude distributions for these revised catalogues are shown in Figure 4.8. The corrections result in increases in activity rate for both the PNR-1z and PNR-2 catalogues. The near linear shift in the magnitudes of the PNR-2 catalogue results in only a small change in the b-value from 1.29 to 1.32. The *b*-value from PNR-1z increases from 1.39 to 1.53 as a result of the gradient of the magnitude conversion relationship. In both cases, the *b*-values remain high.
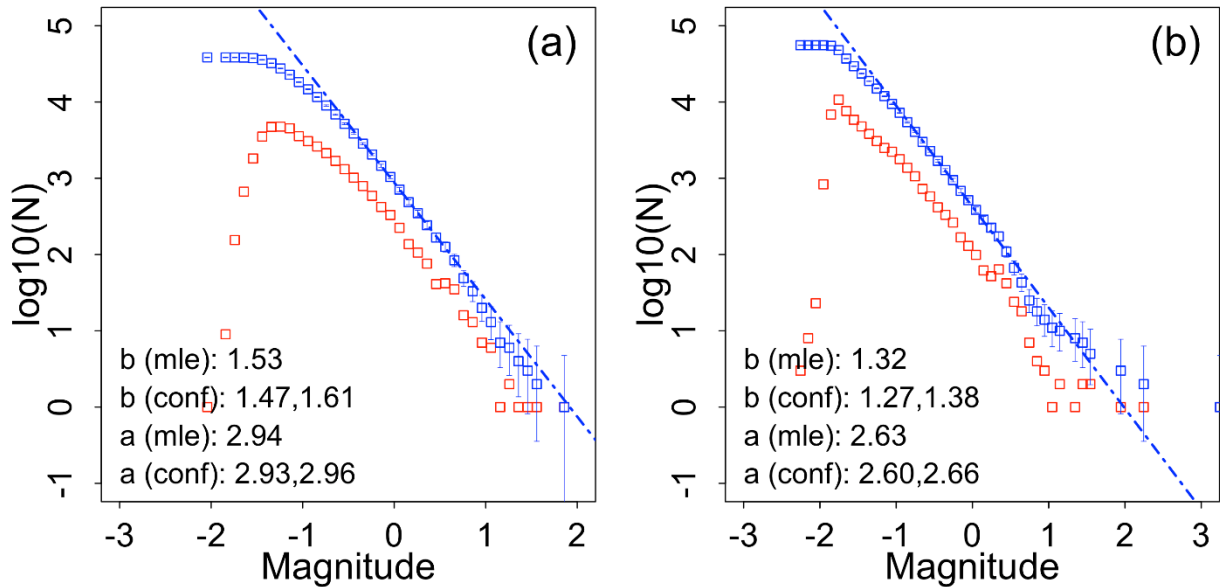

Figure 4.8. Revised frequency magnitude distributions for the downhole catalogues of PNR-1z (a) and PNR-2 (b). Original moment magnitudes are either converted to an equivalent surface moment magnitude using equations (4.6) and (4.7), or for common events, are replaced by the surface moment magnitude from surface recordings.

5 Discussion

Both the downhole and surface catalogues from PNR-1z and PNR-2 suffer from limitations. The roll-off in the frequency magnitude distributions of the downhole catalogues at higher magnitudes together with the overall underestimation of moment magnitude in comparison to surface recordings means that the downhole magnitude estimates reflect only relative size not absolute size. This leads to considerable uncertainty attached to estimates of activity rates and *b*-values and limits the use of the data for reliable estimation of seismic moment release and relating this to operational parameters such as injected volume or injection rate.

We use two different approaches to try to correct the moment magnitudes in the downhole catalogues. In the first approach, we reference the derived relationships between surface local magnitude and downhole moment magnitude to an existing relationship between surface moment magnitude and surface local magnitude. This approach may be suitable where only surface local magnitudes are available and a well-constrained relationship between moment magnitude and local magnitude is already available. The second approach uses a direct relationship between surface and downhole moment magnitudes. This requires both surface and downhole moment magnitudes in sufficient number and quality to be able to derive a robust relationship. Both approaches result in increases in the activity rate measured from frequency-magnitude distributions. However, the two approaches result in differing *b*-values, particularly for PNR-2, where a considerable reduction *b*-value is observed using the first approach. We suggest this may be the result of using two regressions, both of which are uncertain.

While the magnitudes used in the surface catalogues are more reliable, the limited number of events in the catalogues means that the frequency-magnitude distributions are also subject to large

uncertainties as demonstrated by the confidence intervals in the activity rates and *b*-values. This highlights the problem of reliable characterisation of induced seismicity during operations using only surface networks. In particular, the catalogue for PNR-2 may be incomplete around the amber TLS threshold of 0.0 ML, demonstrating the difficulty of meeting existing regulations in high noise environments, even with relatively dense networks of sensors. This seems a minimum requirement. It also precludes the possibility of real-time forecasting with surface networks.

The difference in the ML-Mw scaling between PNR-1z and PNR-2 cannot be easily explained. The same 15 Hz geophones were used in both PNR-1z and PNR-2, though two 3 Hz accelerometers with a lower gain appear to have also been used in PNR-2. The lower gain of the accelerometers may mean that there were more on-scale recordings for the larger events from PNR-2, resulting in less underestimation of magnitude, but lack of individual magnitude estimates for each sensor in the array means it is not possible to assess this fully.

The geophones will also act as a high-pass filters reducing the low frequency spectral plateau of the source displacement spectra. This effect will be most pronounced for the largest events whose corner frequencies are less than the corner frequency of the geophone, resulting in an underestimation of event magnitude. This effect is demonstrated in Figure 5.1, which shows theoretical displacement spectra for different earthquake magnitudes modelled using the Brune (1970) model before, (a), and after filtering with instrument responses with 3 Hz, (b), and 15 Hz, (c), corner frequencies. As the event magnitude increases, the spectral maximum is increasingly reduced and this effect is more pronounced for the 15 Hz response than the 3 Hz one. For this model, the 15 Hz response will start to affect estimates of moment magnitude for events in the magnitude range 0-1 Mw. However, the effect will also be complicated by source parameters such as the stress drop. If the corner frequency remains approximately constant as magnitude varies (e.g. Butcher et al, 2020), this effect will be observed across a wider range of magnitudes.
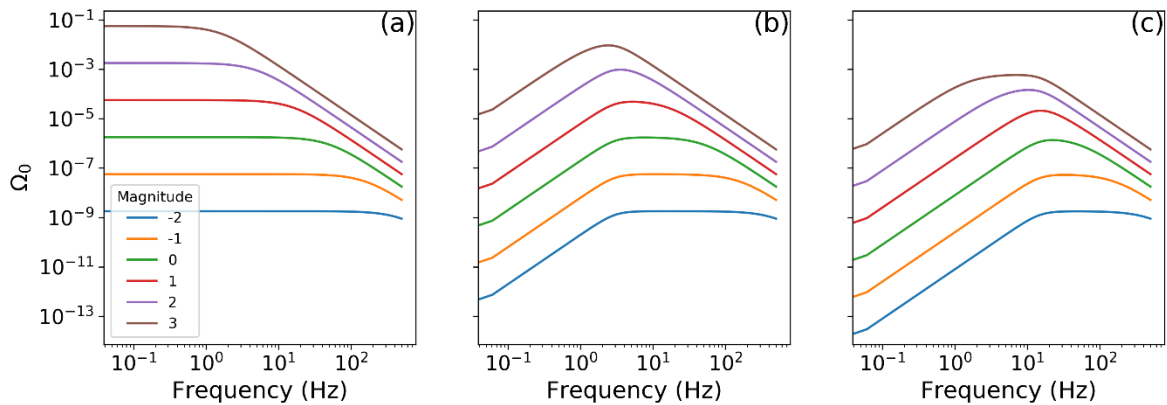
Figure 5.1. (a) Theoretical displacement spectra for different earthquake magnitudes using the Brune (1970) model. Spectra are calculated for a stress drop of 0.1 MPa. (b) and (c) show the same source spectra convolved with the response of sensors with corner frequencies of 3 Hz and 15 Hz respectively.

Overall, both the limited dynamic range and the frequency response of the geophones will reduce the amplitude of the recordings resulting in underestimation of event magnitudes.

This highlights the importance of understanding the effect that instrument type can have on magnitude estimation and also on providing reliable instrument calibration information so that results can be reproduced. Information about the method and parameters is also required to reproduce and asses the reliability of magnitude estimates, otherwise there may be significant differences in the magnitudes obtained using the same input data.

Robust relationships between the different magnitude scales are essential to develop homogeneous and consistent catalogues of seismicity induced during hydraulic fracturing operations. This issue is of particular importance for both deterministic and statistical forecasting of seismicity during operations, which critically depend on robust estimates of seismicity rates and recurrence

parameters. Further work is needed to fully understand the differences between the surface and downhole magnitudes and determine reliable conversion relationships for the PNR-1z and PNR-2 data. This is likely to require calculation of Mw for both downhole catalogues, as well as systematic analysis of the waveform data to understand its limitations.

6 Conclusions

A comparison of the downhole moment magnitudes (Mw) in the PNR-1z and PNR-2 catalogues with local magnitudes (ML) for common events in the surface catalogue shows that the magnitudes from PNR-1z and PNR-2 are not consistent, each having a different Mw-ML relationship. Referencing the ML-Mw data for common events against existing relationships between surface Mw and ML shows that downhole Mw values are significantly less than the expected values of Mw based on surface ML-Mw conversions. This discrepancy is greater for PNR-1z than for PNR-2.

The overall underestimation of moment magnitude in the downhole catalogues may partly be explained by both the limited dynamic range and frequency response of the 15 Hz geophones used in both PNR-1z and PNR-2, leading to magnitude dependent reductions in recorded amplitudes. Such dependence of Mw on recording instruments is clearly undesirable. The use of two low gain accelerometers with a different frequency response in PNR-2 may also have led to differences between magnitude scaling for PNR-1z and PNR-2. However, we are unable to assess this without access to additional data.

Additionally, moment magnitudes calculated from surface recordings of events during operations in PNR-1z and PNR-2 are greater than the moment magnitudes of the same events determined from the downhole data. The former also broadly agree with the moment magnitudes expected from empirical relationships between ML and Mw. Again, this finding may be a result of limited dynamic range and frequency response of the 15 Hz geophones used in the downhole data acquisition. However, it may also reflect differences in the method and parameters used to calculate the moment magnitudes using surface and downhole data as this can also result in significant differences in the resulting magnitudes values.

Although the magnitudes in the surface catalogues do not suffer from the same reliability issues as the downhole ones, the small number of events in the surface catalogues means that there is limited overlap between the surface and downhole catalogues, making it difficult to validate the downhole magnitudes and calculate reliable adjustment factors across a wider range of magnitudes.

Two different approaches were used to correct the moment magnitudes in the downhole catalogues. The first is based on the observed relationship between surface local magnitude and downhole moment magnitude, which is then referenced to an existing relationship between surface moment magnitude and surface local magnitude. The second is based on the observed relationship between surface and downhole moment magnitude. Both approaches result in increases to measured activity rate by correcting the underestimation of moment magnitude in the downhole catalogue. However, the two approaches lead to differing *b*-values, particularly for PNR-2, where a considerable reduction of the *b*-value is observed using the first approach. This may be the result of using two regressions rather than one. As a result, the second approach may be preferable where surface estimates of moment magnitude are available in sufficient number and quality.

A fuller understanding of these results will require calculation of Mw for both the PNR-1z and PNR-2 downhole catalogues, as well as systematic analysis of the waveform data to understand its limitations.

Given these conclusions we suggest the following recommendations for any future operations.

Operators should assess the possible impact of the type of instrumentation on magnitude determination and provide instrument calibration data so that this can also be assessed independently.

The methods and parameters used to calculate magnitudes together with amplitude phase data for individual recording sites are made available to enable duplication of results and assessment of uncertainties.

Denser networks of surface sensors and improved methods of deployment such as shallow borehole sensors should be used to improve event detection and characterisation. This would also help address the limited completeness of the surface catalogues and ensure that all events around amber light threshold of 0 ML are detected.

Moment magnitudes for both the PNR-1z and PNR-2 downhole catalogues should be recalculated, as well as the waveform data systematically analysed to understand its limitations.

7 References

British Geological Survey holds most of the references listed below, and copies may be obtained via the library service subject to copyright legislation (contact libuser@bgs.ac.uk for details). The library catalogue is available at: https://envirolib.apps.nerc.ac.uk/olibcgi.

Aki, K. (1965). Maximum likelihood estimate of b in the formula log N=a-bM and its confidence limits, *Bulletin Earthquake Research Institute, Univ. Tokyo*, 43, 237–239.

Aki K. (1979). Classification of barriers of an earthquake fault, *Journal Geophysical Research*, 84, 6140-6148.

Aki K. & Richards P.G. (2002). *Quantitative Seismology: Theory and Methods*, W.H. Freeman and Co., San Francisco.

Bachmann, C., Wiemer, S., Woessner, J. & Hainzl, S. (2011). Statistical analysis of the induced Basel 2006 earthquake sequence: introducing a probability-based monitoring approach for Enhanced Geothermal Systems, *Geophysical Journal International*, 186, 793-807. https://doi.org/10.1111/j.1365-246X.2011.05068.x.

Bakun, W.H. (1984). Seismic moments, local magnitudes, and coda-duration magnitudes for earthquakes in Central California. *Bulletin of the Seismological Society of America*, 4, 439–458.

Bakun W. & Joyner W.B. (1984). The ML scale in central California, *Bulletin Seismological Society America,* 74, 1827–1843.

Baptie, B. & Luckett, R. (2019), Seismicity induced by hydraulic fracturing operations at Preston New Road, Lancashire, 2018, *Proceedings of the Society for Earthquake and Civil Engineering Dynamics Conference* 2019.

Boore D. & Boatwright J. (1984). Average body-wave correction coefficients. *Bulletin Seismological Society America,* 74, 1615–1621.

Booth, D. (2007). An improved UK local magnitude scale from analysis of shear and Lg-wave amplitudes, *Geophysical Journal International*, 169, 593–601. https://doi.org/10.1111/j.1365-246X.2006.03324.x.

Brune J. N. (1970). Tectonic stress and the spectra of seismic shear waves from earthquakes, *Journal of Geophysical Research*, 75, 4997–5009.

Brune J. N. (1971). Correction, *Journal of Geophysical Research*, 76, 5002.

Butcher, A., Luckett, R., Verdon, J.P, Kendall, J.M., Baptie, B. & Wookey, J. (2017). Local magnitude discrepancies for near-event receivers: Implications for the UK traffic-light scheme,

Bulletin of the Seismological Society of America, 107 (2), 532-541. https://doi.org/10.1785/0120160225.

Butcher, A., Luckett, R.. Kendal. J.-M. & B. Baptie (2020). Corner frequencies, seismic moments and earthquake magnitudes: The effects of high-frequency attenuation on microseismicity. *Bulletin of the Seismological Society of America*

Cao, A.M. & Gao, S.S. (2002). Temporal variations of seismic b-values beneath northeastern japan island arc, *Geophys. Res. Lett.*, 29, https://doi.org/10.1029/2001GL013775.

Chinnery M. A. (1969). Earthquake magnitude and source parameters, *Bulletin of the Seismological Society of America*, 59, 5, 1969–1982.

Clarke, H., Eisner, L., Styles, P. & P. Turner, P. (2014). Felt seismicity associated with shale gas hydraulic fracturing: The first documented example in Europe, *Geophysical Research Letters*, 41, no. 23, 8308–8314. https://doi.org/10.1002/2014GL062047.

Clarke H., Verdon J.P., Kettlety T., Baird A.F. & Kendall J.-M. (2019). Real-Time Imaging, Forecasting, and Management of Human-Induced Seismicity at Preston New Road, Lancashire, England, *Seismol. Res. Lett.*, 90 (5): 1902–1915. https://doi.org/10.1785/0220190110.

Deichmann, N. (2006). Local magnitude, a moment revisited, *Bulletin of the Seismological Society of America*, 96, 1267–1277. https://doi.org/10.1785/0120050115.

Deichmann, N. (2017). Theoretical Basis for the Observed Break in Ml/ Mw Scaling between Small and Large Earthquakes, *Bulletin of the Seismological Society of America*, 107(2), 505–520. https://doi.org/10.1785/0120160318.

Dost, B., Edwards, B., & Bommer, J.J. (2018). The Relationship between M and ML: A Review and Application to Induced Seismicity in the Groningen Gas Field, The Netherlands. Seismological Research Letters, 89(3), 1062–1074. https://doi.org/10.1785/02201700247.

Edwards, B., Allmann, B., Fäh, D., & Clinton, J. (2010). Automatic computation of moment magnitudes for small earthquakes and the scaling of local to moment magnitude. *Geophysical Journal International*, 183(1), 407–420. https://doi.org/10.1111/j.1365-246X.2010.04743.x

Evernden J.F. & Kohler W.M. (1976). Bias in estimates of mb at small magnitudes, *Bulletin of the Seismological Society of America*, **66** (6): 1887-1904.

Fäh, D., Giardini, D., Kästli, P., Deichmann, N., Gisler, M., Schwarz-Zanetti, G., et al. (2011). ECOS-09 Earthquake Catalogue of Switzerland Release 2011. *Report and Database*. Sed/Ecos/R/001/20110417, 1–42.

Goertz-Allmann, B. P., Edwards, B., Bethmann, F., Deichmann, N., Clinton, J., Fäh, D., & Giardini, D. (2011). A new empirical magnitude scaling relation for Switzerland. *Bulletin of the Seismological Society of America*, 101(6), 3088–3095. https://doi.org/10.1785/0120100291

Grünthal, G., Wahlström, R., & Stromeyer, D. (2009). The unified catalogue of earthquakes in central, northern, and northwestern Europe (CENEC)-updated and expanded to the last millennium. *Journal of Seismology*, 13(4), 517–541. https://doi.org/10.1007/s10950-008-9144-9.

Gutenberg, R. & Richter, C.F. (1954). Frequency of earthquakes in California, *Bulletin of the Seismological Society of America*, 34, 185-188.

Hanks, T.C., & Boore, D.M. (1984). Moment-magnitude relations in theory and practice. *Journal of Geophysical Research*, 89(B7), 6229–6235. https://doi.org/10.1029/JB089iB07p06229.

Hanks, T. C., & Kanamori, H. (1979). A moment magnitude scale. *Journal of Geophysical Research*, 84(B5), 2348–2350. https://doi.org/10.1029/JB084iB05p02348

Hutton, L.K. & Boore, D.M. (1987). The ML scale in southern California, *Bulletin Seismological Society America*, 77, 2074–2094.

Cuadrilla Resources Ltd. (2019) Hydraulic Fracture Plan for PNR 2. Available at https://consult.environment-agency.gov.uk/onshore-oil-and-gas/information-on-cuadrillas-preston-new-road-site/user_uploads/pnr-2-hfp-v3.0.pdf

Johnson C, Bittenbinder A, Bogaert B, Dietz L & Kohler, W. (1995). Earthworm: A Flexible Approach to Seismic Network Processing, *IRIS Newsletter*, 14(2): 1-4

Kendall, J.M., Butcher, A., Stork, A.L., Verdon, J.P., Luckett, R. & Baptie, B.J. (2019). How big is a small earthquake? Challenges in determining microseismic magnitudes, *First Break*, 37, 2, 51-56. https://doi.org/10.3997/1365-2397.n0015.

Luckett, R., Ottemöller, L., Butcher, A. & Baptie, B. (2019). Extending local magnitude ML to short distances, *Geophysical Journal International*, 216, 1145-1156, https://doi.org/10.1093/gji/ggy484.

Mancini, S., Segou, M., Werner, M. J. & Baptie, B. J. (2019). *Statistical Modelling of the Preston New Road Seismicity: Towards Probabilistic Forecasting Tools*, Report for OGA.

Munafò, I., Malagnini, L. & Chiaraluce, L. (2016). On the Relationship between Mw and ML for Small Earthquakes, *Bulletin of the Seismological Society of America*, 106. https://doi.org/10.1785/0120160130.

Ottemöller, L. & Havskov, J. (2003). Moment magnitude determination for local and regional earthquakes based on source spectra. *Bulletin of the Seismological Society of America*, 93, 203–214.

Prieto, G.A., Parker, R.L. & F.L. Vernon III (2009). A Fortran 90 library for multitaper spectrum analysis, *Computers and Geosciences*, 35, 1701–1710

Rhoades, D. A. & Dowrick. D.J. (2000). Effects of magnitude uncertainties on seismic hazard estimates. *Proc. 12th World Conference on Earthquake Engineering*, 30 Jan-4 Feb 2000, Wellington, NZ. Paper 1179.

Richter, C.F. (1935). An instrumental earthquake magnitude scale, *Bulletin of the Seismological Society of America*, 25, 1–32.

Ross, Z. E., Ben-Zion, Y., White, M. C. & Vernon, F. L. (2016). Analysis of earthquake body wave spectra for potency and magnitude values: Implications for magnitude scaling relations, *Geophysical Journal International*, 207, no. 2, 1158–1164. https://doi.org/10.1093/gji/ggw327.

Rydelek, P. A. & Sacks, I. S. (1989). Testing the completeness of earthquake catalogs and the hypothesis of self-similarity, *Nature*, 337, 251–253.

Shelly, D.R., Hill, D.P., Massin, F., Farrell, J., Smith, R.B. & Taira, T. (2013). A fluid-driven earthquake swarm on the margin of the Yellowstone caldera, *Journal of Geophysical Research Solid Earth*, 118, 4872–4886. https://doi.org/10.1002/jgrb.50362.

Stork, A., Verdon, J. & Kendall, J.-M. (2014). The robustness of seismic moment and magnitudes estimated using spectral analysis. *Geophysical Prospecting*, 62: 862-878. https://doi.org/10.1111/1365-2478.12134.

Verdon, J. & Budge, J. (2018). Examining the Capability of Statistical Models to Mitigate Induced Seismicity during Hydraulic Fracturing of Shale Gas Reservoirs. *Bulletin of the Seismological Society of America*, 108(2), 690-701. https://doi.org/10.1785/0120170207.

Zaliapin, I. & Ben-Zion, Y. (2015). Artefacts of earthquake location errors and short-term incompleteness on seismicity clusters in southern California. *Geophysical Journal International*, 202(3), 1949–1968, https://doi.org/10.1093/gji/ggv259.